Derivation of the ghost Gutzwiller approximation from quantum embedding principles: Ghost density matrix embedding theory

Nicola Lanatà ®*

School of Physics and Astronomy, Rochester Institute of Technology, 84 Lomb Memorial Drive, Rochester, New York 14623, USA
and Center for Computational Quantum Physics, Flatiron Institute, New York, New York 10010, USA

Establishing the underlying links between the diverse landscape of theoretical frameworks for simulating strongly correlated matter is crucial for advancing our understanding of these systems. In this work, we focus on the ghost Gutzwiller approximation (gGA), an extension of the Gutzwiller approximation (GA) based on the variational principle. We derive a framework called "ghost density matrix embedding theory" (gDMET) from quantum embedding (QE) principles similar to those in density matrix embedding theory (DMET), which reproduces the gGA equations for multiorbital Hubbard models with a simpler implementation. This derivation highlights the crucial role of the ghost degrees of freedom, not only as an extension to the GA, but also as the key element in establishing a consistent conceptual connection between DMET and the gGA. This connection further elucidates how gGA overcomes the systematic accuracy limitations of standard GA and achieves results comparable to dynamical mean field theory. Furthermore, it offers an alternative interpretation of the gGA equations, fostering new ideas and generalizations.

DOI: 10.1103/PhysRevB.108.235112

I. INTRODUCTION

Theoretical frameworks based on quantum embedding (QE) principles [1,2] have emerged as powerful tools for studying strongly correlated matter. Among these, dynamical mean field theory (DMFT) [3–7] is a well-known and widely used method. Other methods, such as the Gutzwiller approximation (GA) [8–15], its recent extension to ghost GA (gGA) [16–18], the rotationally invariant slave boson (RISB) theory [19–21], the slave spin theory [22,23], and density matrix embedding theory (DMET) [24–32], have also made significant contributions. In this work, we focus on GA and gGA, both of which are based on the variational principle and, as DMFT, on the limit of infinite dimensionality [8,9].

The key idea underlying gGA is to expand the GA variational space by incorporating auxiliary "ghost" fermionic degrees of freedom—which is a common theme with different frameworks such as extensions to DMET [33,34], matrix product states and projected entangled pair states [35], the ancilla qubit technique [36], and recent extensions of neural network states [37]. It also presents suggestive analogies with the concepts of "hidden fermion" [38] and "hidden Fermi liquid" [39].

The gGA variational extension allows one to achieve an accuracy comparable to that of DMFT, but with a substantially lower computational cost [16,17,40,41]. Additionally, the gGA, like the GA, can be reformulated using a RISB perspective [42–45], providing us with an exact reformulation of the many-body problem that reduces to gGA at the mean field level. This alternative formulation may pave the way to develop practical implementations for systematically adding quantum-fluctuation corrections towards the exact solution.

In Refs. [13,16,17], it was shown that the GA and gGA can both be formulated using a typical QE algorithmic structure, analogous to DMET. This structure involves the recursive computation of an embedding Hamiltonian's (EH's) ground state for each correlated fragment of the system. In practice, this approach offers new opportunities to reduce the computational costs of GA and gGA—e.g., by employing density matrix renormalization group [46], variational quantum eigensolvers [47–49], or other classical methods [50,51], to compute the EH's ground state. Subsequently, the comparison between the GA and DMET equations was also discussed in Refs. [52,53], where it was noted that the main mathematical difference between the DMET and the GA, as formulated in Refs. [13,21] using a QE structure, is that the latter involves variational parameters encoding the quasiparticle spectral weights of the correlated degrees of freedom, which are effectively set to 1 in DMET.

The mathematical similarities between GA, gGA, and DMET algorithms, outlined above, suggest a possible underlying physical connection between these methods. However, such a connection has not been established yet.

In this paper, we address this issue by deriving the ghost DMET (gDMET): a QE method based on principles similar to those of DMET, possessing self-consistency conditions mathematically equivalent to those found in the gGA variational-energy minimization framework [16,17]. This clear correspondence between gGA and gDMET offers a valuable alternative perspective on interpreting the physical implications of the resulting equations and introduces a practical advantage with a simpler implementation. Furthermore, as our approach yields nonarbitrary self-consistency

*Corresponding author: nxlsps@rit.edu

conditions consistent with the variational principle in the infinite-dimensional limit, it could serve as a guide for developing new QE methods with enhanced accuracy and broader applicability, e.g., for systems with nonlocal interactions [54–59], at finite temperature [60–63], and out of equilibrium [64–71].

II. DERIVATION OF gDMET: THE gGA FROM QE SELF-CONSISTENCY PRINCIPLES

Let us consider a generic multiorbital Fermi-Hubbard Hamiltonian represented as follows:

$$\hat{H} = \sum_{i=1}^{\mathcal{N}} \hat{H}_{\text{loc}}^i [c_{i\alpha}^\dagger, c_{i\alpha}] + \sum_{i \neq j} \hat{T}_{ij}, \tag{1}$$

$$\hat{T}_{ij} = \sum_{\alpha=1}^{\nu_i} \sum_{\beta=1}^{\nu_j} [t_{ij}]_{\alpha\beta} c_{i\alpha}^\dagger c_{j\beta}, \tag{2}$$

where i and j label the fragments of the system, $\hat{H}_{\text{loc}}^i$ is a generic operator lying within the i fragment (i.e., constructed with $c_{i\alpha}^\dagger, c_{i\alpha}$), including both one-body and two-body contributions, and α labels all fermionic modes within each fragment.

The key idea underlying QE frameworks is to describe the interaction of each fragment i with its environment in terms of an EH $\hat{H}_{\text{emb}}^i$, consisting of the fragment and an entangled quantum bath. In principle, it can be demonstrated that the fragments can always be exactly embedded by baths no larger than the fragments themselves [24,25]. However, this result is purely formal. In DMET, a practical approximation to the bath of $\hat{H}_{\text{emb}}^i$ is built from a one-body state, which is generally constructed as the ground state of an auxiliary one-body Hamiltonian $\hat{H}_*$ determined by appropriate self-consistency conditions, rather than the original interacting Hamiltonian $\hat{H}$.

The goal of this section is to develop the gGA from QE self-consistency principles reminiscent of DMET. Like gGA and the DMET frameworks of Refs. [33,34], our construction will involve an effective one-body Hamiltonian $\hat{H}_*$ featuring auxiliary fermionic degrees of freedom, which will serve to enrich the description of many-body effects compared to classical DMET frameworks.

A. The gDMET quasiparticle Hamiltonian

In our approach, we construct the effective Hamiltonian $\hat{H}_*$, also called "quasiparticle Hamiltonian," as in the gGA literature,

$$\hat{H}_*[\mathcal{R}, \Lambda] = \sum_{i=1}^{\mathcal{N}} \sum_{a,b=1}^{B\nu_i} [\Lambda_i]_{ab} f_{ia}^\dagger f_{ib} + \sum_{i \neq j} \hat{T}_{ij},$$

$$\hat{T}_{ij} = \sum_{a=1}^{B\nu_i} \sum_{b=1}^{B\nu_j} [\mathcal{R}_i t_{ij} \mathcal{R}_j^\dagger]_{ab} f_{ia}^\dagger f_{jb}, \tag{3}$$

where $\mathcal{R} = (\mathcal{R}_1, \dots, \mathcal{R}_{\mathcal{N}})$, $\Lambda = (\Lambda_1, \dots, \Lambda_{\mathcal{N}})$, we assume that $B > 1$ is an odd number, and we introduced modes $f_{ia}^\dagger$, with original fermionic modes $c_{i\alpha}^\dagger$ expressed as linear
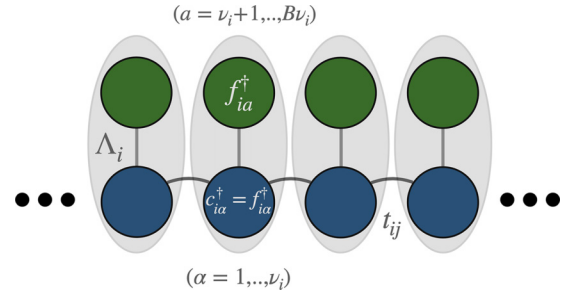
FIG. 1. Schematic one-dimensional representation of the effective Hamiltonian $\hat{H}_*$ in the ideal scenario described in Sec. II A. The physical degrees of freedom $c_{i\alpha}^\dagger = f_{i\alpha}^\dagger$, $\alpha = 1, \dots, \nu_i$, are represented by blue circles. The additional ghost modes $f_{ia}^\dagger$, $a = \nu_i + 1, \dots, B\nu_i$, are represented by green circles.

combinations,

$$c_{i\alpha}^\dagger = \sum_{a=1}^{B\nu_i} [\mathcal{R}_i]_{a\alpha} f_{ia}^\dagger \quad (\alpha = 1, \dots, \nu_i). \tag{4}$$

Note that $\hat{T}_{ij}$ is the same operator in Eqs. (2) and (3), as it can be readily verified by substituting Eq. (4) in Eq. (2).

Similarly to all DMET implementations, the entries of the parameters Λ_i and $\mathcal{R}_i$ characterizing $\hat{H}_*$ are initially unspecified, and will be determined self-consistently.

For Eq. (4) to be logically coherent and provide $c_{i\alpha}^\dagger$ and $f_{ia}^\dagger$ modes, both satisfying canonical anticommutation rules

$$\{f_{ia}, f_{jb}^\dagger\} = \delta_{ij}\delta_{ab}, \tag{5}$$

$$\{c_{i\alpha}, c_{j\beta}^\dagger\} = \delta_{ij}\delta_{\alpha\beta}, \tag{6}$$

the condition $\mathcal{R}_i^\dagger \mathcal{R}_i = \mathbf{1}$ (where $\mathbf{1}$ is the identity matrix) has to hold true, as it can be verified by substituting Eq. (4) in Eq. (6) and comparing the resulting equation with Eq. (5). When this condition is exactly satisfied, the modes $f_{ia}^\dagger$ can be chosen in such a way that $[\mathcal{R}_i]_{a\alpha} = \delta_{a\alpha} \; \forall a, \alpha \leqslant \nu_i$, and $[\mathcal{R}_i]_{a\alpha} = 0$ otherwise.

This ideal scenario, corresponding to the system represented in Fig. 1, is useful for interpreting the gGA equations from a DMET perspective. Specifically, it allows interpreting $\hat{H}_*$ as an effective Hamiltonian approximating many-body interactions between fragments and their environments using one-body operators; with "hopping" (nonlocal) terms retained as in the original Hamiltonian $\hat{H}$, and new "ghost" or "ancilla" fermionic degrees of freedom introduced locally in all fragments to enrich the approximate description of many-body effects induced by local interacting terms of $\hat{H}$.

For later convenience, we rewrite Eq. (3) as follows:

$$\hat{H}_*[\mathcal{R}, \Lambda] = \sum_{i,j=1}^{\mathcal{N}} [\Pi_i h_* \Pi_j]_{ab} f_{ia}^\dagger f_{jb}, \tag{7}$$

where we introduced the matrix

$$h_* = \begin{pmatrix} \Lambda_1 & \mathcal{R}_1 t_{12} \mathcal{R}_2^\dagger & \dots & \mathcal{R}_1 t_{1\mathcal{N}} \mathcal{R}_{\mathcal{N}}^\dagger \\ \mathcal{R}_2 t_{21} \mathcal{R}_1^\dagger & \Lambda_2 & \dots & \vdots \\ \vdots & \vdots & \ddots & \vdots \\ \mathcal{R}_{\mathcal{N}} t_{\mathcal{N}1} \mathcal{R}_1^\dagger & \dots & \dots & \Lambda_{\mathcal{N}} \end{pmatrix}, \tag{8}$$

and the projectors over the degrees of freedom corresponding to each fragment

$$\Pi_i = \begin{pmatrix} \delta_{i1}[\mathbf{1}]_{B\nu_1 \times B\nu_1} & \cdots & \mathbf{0} \\ \vdots & \ddots & \vdots \\ \mathbf{0} & \cdots & \delta_{iM}[\mathbf{1}]_{B\nu_M \times B\nu_M} \end{pmatrix}, \quad (9)$$

where $[\mathbf{1}]_{n \times n}$ is the $n \times n$ identity matrix.

B. Construction of the EH

As previously outlined, our objective is to employ the Hamiltonian $\hat{H}_*$ to form an EH, denoted by $\hat{H}_{\mathrm{emb}}^i$, to approximate the interaction of each fragment i with its surrounding environment within the original system $\hat{H}$. In this section, we delineate the specific methodical process of building the EH within the DMET framework under development in this study.

For this purpose, we leverage on a general theorem based on the Schmidt decomposition, here provided in the Supplemental Material for completeness [72]. This theorem, a standard result in DMET frameworks [74], allows one to express the so-called "active part" of the ground state $|\Psi_0\rangle$ of $\hat{H}_*$ [see Eq. (3)] for each fragment i. With the "active part," here we refer to the part of $|\Psi_0\rangle$ constructed from the $B\nu_i$ $f_{ia}^\dagger$ modes and the $B\nu_i$ modes entangled with it, while the "inactive part" refers to the part of $|\Psi_0\rangle$ constructed with the remaining fermionic modes, which is entirely decoupled from the i fragment and the corresponding active part of the ground state. Specifically, the theorem demonstrates that the active part corresponds to the ground state of a one-body EH involving $B\nu_i$ fragment degrees of freedom, denoted as $f_{ia}^\dagger$, and $B\nu_i$ "bath" degrees of freedom entangled with it, denoted as $b_{ia}^\dagger$, given by the following equation:

$$b_{ia}^\dagger = \sum_{j=1}^{\mathcal{N}} \sum_{b=1}^{B\nu_j} [\mathcal{B}_i^j]_{ba} f_{jb}^\dagger \quad (a = 1, \ldots, B\nu_i), \quad (10)$$

where the entries of the matrices $\mathcal{B}_i^j$ are given by the following equation:

$$[\mathcal{B}_i^j]_{ba} = (1 - \delta_{ij}) \left[\Pi_j f(h_*) \Pi_i \frac{1}{\sqrt{{}^t\Delta_i (\mathbf{1} - {}^t\Delta_i)}} \right]_{ba}, \quad (11)$$

where

$$[\Delta_i]_{ab} = \langle \Psi_0 | f_{ia}^\dagger f_{ib} | \Psi_0 \rangle \quad (a, b = 1, \ldots, B\nu_i), \quad (12)$$

$f(h_*)$ is the Fermi function of the matrix h_*, and ${}^t\Delta_i$ indicates the transpose of Δ_i. For later convenience, we also define the following matrix:

$$\mathcal{B}_i = \sum_{j=1}^{\mathcal{N}} \mathcal{B}_i^j. \quad (13)$$

As explained in the Supplemental Material [72], it is possible to project $\hat{H}_*$ onto the space spanned by the "active" degrees of freedom associated to each fragment i. The resulting one-body embedding Hamiltonian is the following:

$$\hat{H}_0^i = \sum_{a,b=1}^{B\nu_i} [\Lambda_i]_{ab} f_{ia}^\dagger f_{ib} - \sum_{a,b=1}^{B\nu_i} [\Lambda_i^c]_{ab} b_{ia}^\dagger b_{ib}$$
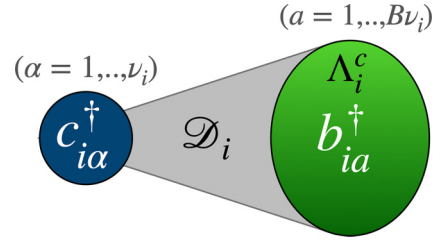
FIG. 2. Schematic representation of the EH $\hat{H}_{\mathrm{emb}}^i$. The fragment degrees of freedom $c_{i\alpha}^\dagger$, $\alpha = 1, \ldots, \nu_i$, are represented by a blue circle, while the additional bath modes $f_{ia}^\dagger$, $a = 1, \ldots, B\nu_i$, are represented by a green ellipse. The matrix Λ_i^c encodes the bath degrees of freedom and the ghost modes, while the matrix $\mathcal{D}_i$ encodes the hybridization with the fragment.

$$+ \sum_{a,b=1}^{B\nu_i} ([\mathcal{D}_i^0]_{ba} f_{ia}^\dagger b_{ib} + \mathrm{H.c.})$$

$$= \sum_{a,b=1}^{B\nu_i} [\Lambda_i]_{ab} f_{ia}^\dagger f_{ib} - \sum_{a,b=1}^{B\nu_i} [\Lambda_i^c]_{ab} b_{ia}^\dagger b_{ib}$$

$$+ \sum_{a,b=1}^{B\nu_i} \sum_{\alpha=1}^{\nu_i} ([\mathcal{D}_i]_{b\alpha} c_{i\alpha}^\dagger b_{ib} + \mathrm{H.c.}), \quad (14)$$

where

$$[\Lambda_i^c]_{ab} = -[\Pi_i \mathcal{B}_i^\dagger h_* \mathcal{B}_i \Pi_i]_{ab}, \quad (15)$$

$$[\mathcal{D}_i^0]_{ba} = [\Pi_i h_* \mathcal{B}_i]_{ab} = \sum_j [\mathcal{R}_i t_{ij} \mathcal{R}_j^\dagger \mathcal{B}_i^j]_{ab}, \quad (16)$$

$$[\mathcal{D}_i]_{ba} = \sum_j [t_{ij} \mathcal{R}_j^\dagger \mathcal{B}_i^j]_{ab}, \quad (17)$$

and in the last step of Eq. (14), we used Eq. (4).

Given $\hat{H}_0^i$, we construct the following approximation to the actual EH of each impurity for the original interacting Hamiltonian $\hat{H}$ [Eq. (1)] as follows:

$$\hat{H}_{\mathrm{emb}}^i = \hat{H}_0^i - \sum_{a,b=1}^{B\nu_i} [\Lambda_i]_{ab} f_{ia}^\dagger f_{ib} + \hat{H}_{\mathrm{loc}}^i [c_{i\alpha}^\dagger, c_{i\alpha}]$$

$$= \hat{H}_{\mathrm{loc}}^i [c_{i\alpha}^\dagger, c_{i\alpha}] - \sum_{a,b=1}^{B\nu_i} [\Lambda_i^c]_{ab} b_{ia}^\dagger b_{ib}$$

$$+ \sum_{a,b=1}^{B\nu_i} \sum_{\alpha=1}^{\nu_i} ([\mathcal{D}_i]_{b\alpha} c_{i\alpha}^\dagger b_{ib} + \mathrm{H.c.}), \quad (18)$$

which is schematically reproduced in Fig. 2.

This working hypothesis, which will enable us to recover the gGA equations, can be physically motivated by noting that the fragment portion of the EH is already known to be $\hat{H}_{\mathrm{loc}}^i$. Therefore, that part does not need to be approximated.

C. Calculating the ground state of the EH

It is essential to recognize that $\hat{H}_{\mathrm{emb}}^i$ explicitly involves only the ν_i fragment modes $c_{i\alpha}^\dagger$ and the $B\nu_i$ bath modes $b_{ia}^\dagger$, but exists within the extended Hilbert space containing all $2B\nu_i$ degrees of freedom. This space includes both the "physical"

$(B+1)\nu_i$ modes in Eq. (18) and the "unphysical" $(B-1)\nu_i$ modes decoupled from it. Consequently, the ground state of $\hat{H}^i_{\text{emb}}$ is a tensor product of a "physical" state and an "unphysical" state, with the latter not affecting the expectation value of $\hat{H}^i_{\text{emb}}$.

It is also important to note that projecting $\hat{H}_*$ into the ith "active space" leads to the total EH system [including the additional $(B-1)\nu_i$ auxiliary modes] being half filled, i.e., containing $B\nu_i$ fermions in total, as explained in the Supplemental Material [72].

From the observations above, it follows that calculating the ground state of $\hat{H}^i_{\text{emb}}$ requires separately inspecting the blocks corresponding to various assignments of the available $B\nu_i$ fermions between the auxiliary modes and the physically relevant portion of the EH, and identifying the one with lowest energy.

Interestingly, a similar challenge is encountered in gGA [16]. Here, different assignments of fermions lead to various variational states, with the physical solution having the lowest variational energy. Previous gGA work indicates that the lowest-energy solution is obtained when the physically relevant portion of the EH, corresponding to the $(B+1)\nu_i$ modes in Eq. (18), is half filled with $\nu_i(B+1)/2$ fermions (integer for odd B, as assumed in Sec. II A). This observation, highlighted in Ref. [17], significantly reduces the computational cost and will also be exploitable in DMET, within the context of the gDMET framework that we are in the process of explaining in this paper.

D. Self-consistency conditions

We now postulate the following self-consistency conditions for determining the parameters $\mathcal{R}_i$ and Λ_i:

$$\langle\Psi_0[\mathcal{R},\Lambda]|\,b^\dagger_{ia}b_{ib}\,|\Psi_0[\mathcal{R},\Lambda]\rangle = \langle\Phi_i|\,b^\dagger_{ia}b_{ib}\,|\Phi_i\rangle, \quad (19)$$

$$\langle\Psi_0[\mathcal{R},\Lambda]|\,c^\dagger_{i\alpha}b_{ib}\,|\Psi_0[\mathcal{R},\Lambda]\rangle = \langle\Phi_i|\,c^\dagger_{i\alpha}b_{ib}\,|\Phi_i\rangle, \quad (20)$$

where $|\Psi_0\rangle$ is the ground state of $\hat{H}_*$ and $|\Phi_i\rangle$ is the ground state of $\hat{H}^i_{\text{emb}}$; see Eq. (18).

This working hypothesis, which will allow us to recover the gGA equations, can be physically motivated by observing that the role of $|\Psi_0\rangle$ is to approximate the environment of each fragment and its interaction with the fragment itself, which are directly related to Eqs. (19) and (20), respectively.

Note that as shown in the Supplemental Material [72], the left-hand side of Eq. (19) is given by

$$\langle\Psi_0[\mathcal{R},\Lambda]|\,b^\dagger_{ia}b_{ib}\,|\Psi_0[\mathcal{R},\Lambda]\rangle = [\mathbf{1}-\Delta_i]_{ab}. \quad (21)$$

Similarly, the left-hand side of Eq. (20) is given by the following equation:

$$\langle\Psi_0[\mathcal{R},\Lambda]|\,c^\dagger_{i\alpha}b_{ib}\,|\Psi_0[\mathcal{R},\Lambda]\rangle$$
$$= \sum_{a=1}^{B\nu_i}[\mathcal{R}_i]_{a\alpha}\langle\Psi_0[\mathcal{R},\Lambda]|\,f^\dagger_{ia}b_{ib}\,|\Psi_0[\mathcal{R},\Lambda]\rangle$$
$$= \sum_{a=1}^{B\nu_i}[\mathcal{R}_i]_{a\alpha}[\Delta_i(\mathbf{1}-\Delta_i)]^{\frac{1}{2}}_{ab}. \quad (22)$$

E. Summary

In summary, the solution to the gDMET quantum embedding problem is given by the following identities:

$$\hat{H}_*[\mathcal{R},\Lambda]|\Psi_0\rangle = E_0|\Psi_0\rangle, \quad (23)$$

$$[\Delta_i]_{ab} = \langle\Psi_0|\,f^\dagger_{ia}f_{ib}\,|\Psi_0\rangle, \quad (24)$$

$$\mathcal{B}^j_i = (1-\delta_{ij})\,\Pi_j\,f(h_*)\Pi_i\frac{1}{\sqrt{{}^t\Delta_i(\mathbf{1}-{}^t\Delta_i)}}, \quad (25)$$

$$\mathcal{B}_i = \sum_{j=1}^{\mathcal{N}}\mathcal{B}^j_i, \quad (26)$$

$$[\mathcal{D}_i]_{b\alpha} = \sum_{j=1}^{\mathcal{N}}[t_{ij}\mathcal{R}^\dagger_j\mathcal{B}^j_i]_{\alpha b}, \quad (27)$$

$$[\Lambda^c_i]_{ab} = -[\Pi_i\mathcal{B}^\dagger_i h_*\mathcal{B}_i\Pi_i]_{ab}, \quad (28)$$

$$\hat{H}^i_{\text{emb}}|\Phi_i\rangle = E^c_i|\Phi_i\rangle, \quad (29)$$

$$\langle\Phi_i|\,b^\dagger_{ia}b_{ib}\,|\Phi_i\rangle = [\mathbf{1}-\Delta_i]_{ab}, \quad (30)$$

$$\langle\Phi_i|\,c^\dagger_{i\alpha}b_{ib}\,|\Phi_i\rangle = \sum_{a=1}^{B\nu_i}[\mathcal{R}_i]_{a\alpha}[\Delta_i(\mathbf{1}-\Delta_i)]^{\frac{1}{2}}_{ab}, \quad (31)$$

where the embedding parameters Λ^c_i and Δ_i, characterizing the EH $\hat{H}^i_{\text{emb}}$ of the fragments, depend on $\mathcal{R}_i$ and Λ_i through the steps described above; Eq. (29) consists in computing the ground state of $\hat{H}^i_{\text{emb}}$; and Eqs. (30) and (31) are the self-consistency conditions to be satisfied for determining $\mathcal{R}_i$ and Λ_i.

In the Supplemental Material, we provide a proof that the gDMET equations presented above are indeed mathematically equivalent to the gGA equations [72]. This equivalence allows for a complementary physical interpretation. Furthermore, our approach introduces a practical advantage, as Eq. (28) offers a simpler method for calculating Λ^c_i compared to the expression used in previous GA/gGA implementations [72].

A key mathematical distinction of our approach, compared to other DMET implementations proposed in the literature, is that Eqs. (23)–(31) do not form an under-determined system, but can be exactly satisfied simultaneously. The primary reason is that the combined number of independent entries of Λ_i and $\mathcal{R}_i$ is equal to the number of independent EH density matrix elements appearing in the left-hand sides of Eqs. (30) and (31). In classic DMET frameworks, however, the matrices $\mathcal{R}_i$ are not considered as free parameters, and the parameters Λ_i are insufficient for exactly satisfying the QE self-consistency conditions. The standard DMET approach to tackle this problem is to address the self-consistency conditions only approximately, with respect to an arbitrary notion of distance. On the other hand, the QE framework derived in this work relies on the assumption that the matrices $\mathcal{R}_i$ satisfy the condition $\mathcal{R}^\dagger_i\mathcal{R}_i = \mathbf{1}$, which should therefore be interpreted as a "sanity check" of the theory, but is not generally exactly verified. The discrepancy between the ideal assumption of $\mathcal{R}^\dagger_i\mathcal{R}_i = \mathbf{1}$ and the actual matrix conditions found in practice hints at a common underlying physical reason that is relevant to both our approach and the classic DMET frameworks.

From a physical standpoint, this common underlying physical reason can be traced back to the role of the ghost degrees of freedom. In classic GA (i.e., for $B = 1$, corresponding to the limiting case without ghost fermionic degrees of freedom), $\mathcal{R}_i^\dagger \mathcal{R}_i = \mathcal{Z}_i$ represents the quasiparticle weight of the i degrees of freedom. Since generally the eigenvalues of $\mathcal{Z}_i$ are smaller than 1, the QE procedure above becomes less justified in the correlated regime from a DMET perspective (while it remains perfectly justified from the GA variational perspective). In contrast, gGA incorporates ghost fermionic degrees of freedom, where $\mathcal{R}_i^\dagger \mathcal{R}_i$ represents the entire spectral weight of the i degrees of freedom, including both the quasiparticle weight and the contribution of the Hubbard bands. Therefore, in gGA, one generally finds that $\mathcal{R}_i^\dagger \mathcal{R}_i \sim \mathbf{1}$ in all physical regimes, ranging from the weakly correlated to the strongly correlated. This fact can be interpreted as an *a posteriori* indication that the additional ghost degrees of freedom allow us to capture, with higher precision, the many-body effects induced by local interacting terms of $\hat{H}$, justifying our procedure.

In light of the above discussion, we argue that the ghost degrees of freedom play a pivotal role in unifying the DMET and gGA perspectives, offering a common framework that successfully captures many-body effects, while adhering to the principles of both approaches.

III. GAUGE FREEDOM AND QE GAUGE FROM SINGULAR VALUE DECOMPOSITION

In this section, we discuss the gauge invariance of the equations derived in our paper. By inspection, one can verify that Eqs. (24)–(31) are invariant with respect to the following set of gauge transformations:

$$|\Psi_0\rangle \rightarrow \hat{\mathcal{U}}^\dagger(\theta_1, \ldots, \theta_\mathcal{N})|\Psi_0\rangle, \tag{32}$$

$$|\Phi_i\rangle \rightarrow \hat{U}_i^\dagger(\theta_i)|\Phi_i\rangle, \tag{33}$$

$$\mathcal{R}_i \rightarrow u_i^\dagger(\theta_i)\mathcal{R}_i, \tag{34}$$

$$\mathcal{D}_i \rightarrow {}^t u(\theta_i)\mathcal{D}_i, \tag{35}$$

$$\Delta_i \rightarrow {}^t u_i(\theta_i)\Delta_i {}^t u_i^\dagger(\theta_i), \tag{36}$$

$$\Lambda_i \rightarrow u_i^\dagger(\theta_i)\Lambda_i u_i(\theta_i), \tag{37}$$

$$\Lambda_i^c \rightarrow u_i^\dagger(\theta_i)\Lambda_i^c u_i(\theta_i), \tag{38}$$

where θ_i are Hermitian matrices of Lie parameters and

$$u_i(\theta_i) = e^{i\theta_i}, \tag{39}$$

$$\hat{U}_i(\theta_i) = e^{i\sum_{a,b=1}^{Bv_i}[\theta_i]_{ab}b_{ia}^\dagger b_{ib}}, \tag{40}$$

$$\hat{\mathcal{U}}(\theta_1, \ldots, \theta_\mathcal{N}) = e^{i\sum_i\sum_{a,b=1}^{Bv_i}[\theta_i]_{ab}f_{ia}^\dagger f_{ib}}. \tag{41}$$

In the context of our derivation of the QE equations, the invariance under the given set of gauge transformations stems from the fact that the choice of the f_{ia} modes is arbitrary, as long as they can span the physical $c_{i\alpha}$ modes. The term "gauge" refers to the idea that such a basis choice does not impact physical quantities since all parameters related by this group of transformations are effectively equivalent. In

particular, note that Eq. (33) corresponds to applying any unitary transformation to the bath of the effective Hamiltonian, which does not affect the expectation values of fragment observables in the EH (as in DMFT).

Importantly, as discussed in Sec. II A, if the identity $\mathcal{R}_i^\dagger \mathcal{R}_i = \mathbf{1}$ was exactly satisfied, we would be able to choose a gauge that corresponds to the ideal scenario depicted in Fig. 1– which was used to justify our QE procedure. On the other hand, even when $\mathcal{R}_i^\dagger \mathcal{R}_i = \mathbf{1}$ is verified only approximately, we can leverage the gauge freedom to transform $\mathcal{R}_i$ into a form that closely resembles the ideal scenario depicted in Fig. 1 (which we are going to refer to as the "QE gauge"). To illustrate this point, we will present an argument based on the singular value decomposition (SVD) of $\mathcal{R}_i$.

The SVD theorem states that it is always possible to express a rectangular matrix such as $\mathcal{R}_i$ as follows:

$$\mathcal{R}_i = U_i\Sigma_i V_i^\dagger, \tag{42}$$

where U_i is a $Bv_i \times Bv_i$ matrix, V_i is a $v_i \times v_i$ unitary matrix, and Σ_i is a $Bv_i \times v_i$ diagonal matrix, where $[\Sigma_i]_{\alpha\alpha} \geqslant 0$ $\forall \alpha \leqslant v_i$ are the "singular values," and $[\Sigma_i]_{aa} = 0$ $\forall a > v_i$. This property arises from the fact that the SVD captures the effective rank of $\mathcal{R}_i$, which is v_i, and the nonzero singular values correspond to the contributions from the physical $c_{i\alpha}$ modes. In our context of application inherent in the gGA equations, where we know that

$$\mathcal{R}_i^\dagger \mathcal{R}_i \simeq \mathbf{1} \tag{43}$$

is accurately satisfied, we have that $[\Sigma_i]_{aa} \simeq \delta_{a\alpha}$ for $a \leqslant v_i$, as can be readily verified by noting that

$$\Sigma_i^\dagger \Sigma_i = V_i^\dagger \mathcal{R}_i^\dagger \mathcal{R}_i V_i. \tag{44}$$

Let us define the gauge transformation $u_i = U_i\bar{V}_i^\dagger$, where $\bar{V}_i$ is a unitary block matrix with entries $[\bar{V}_i]_{\alpha\beta} = [V_i]_{\alpha\beta}\forall \alpha, \beta \leqslant v_i$, $[\bar{V}_i]_{ab} = \delta_{ab}\forall a, b \geqslant v_i + 1$, and 0 elsewhere. By applying such gauge transformation to $\mathcal{R}_i$, we can bring it into a form close to the one corresponding to the ideal scenario of Fig. 1. In fact,

$$\mathcal{R}_i' = u_i^\dagger \mathcal{R}_i = \bar{V}_i\Sigma_i V_i, \tag{45}$$

which has entries

$$[\mathcal{R}_i']_{\alpha\beta} \simeq \delta_{\alpha\beta}, \qquad \forall \alpha, \beta \leqslant v_i, \tag{46}$$

$$[\mathcal{R}_i']_{a\alpha} = 0, \qquad \forall a > v_i, \tag{47}$$

where Eq. (46) holds true because the corresponding block of $\mathcal{R}_i'$ consists of a unitary rotation of the singular values of Σ_i, which we know to be approximately 1 under our hypothesis; see Eqs. (43) and (44).

In the arguments presented above, it is important to emphasize that the construction allowing us to obtain an $\mathcal{R}_i$ matrix with the ideal form depicted in Fig. 1 is specifically applicable only to the gGA framework, where $B > 1$, as our key hypothesis that $\mathcal{R}_i^\dagger \mathcal{R}_i \simeq \mathbf{1}$ is not satisfied in the case of the classic GA with $B = 1$.

In the following section, we will provide a concrete illustration of the gauge-fixing construction explained above. Specifically, we will apply these concepts to the simple case of the Hubbard model at particle-hole symmetry, within the gGA

framework with $B = 3$, as previously studied in Ref. [16]. This example will serve to further clarify the gauge-fixing procedure and demonstrate the practical utility of the auxiliary ghost modes in capturing the many-body effects arising in this system.

QE gauge fixing for single-band Hubbard model

Let us consider the special case of a single-band Hubbard model ($\nu_i = 1$) satisfying particle-hole symmetry and translational invariance. The translational invariance implies that $\mathcal{R}_i = \mathcal{R}$ and $\Lambda_i = \Lambda$ are independent of the fragment i. Furthermore, as previously pointed out in Ref. [16], the particle-hole symmetry condition implies that in the gauge that diagonalizes Λ, we have

$$\mathcal{R} = \begin{pmatrix} \sqrt{z} \\ \sqrt{h/2} \\ \sqrt{h/2} \end{pmatrix}, \qquad \Lambda = \begin{pmatrix} 0 & 0 & 0 \\ 0 & l & 0 \\ 0 & 0 & -l \end{pmatrix}, \quad (48)$$

where z represents the quasiparticle weight, h represents the spectral weight of the Hubbard bands, and l controls the position of the Hubbard bands.

In such simple case, the SVD of $\mathcal{R}$,

$$\mathcal{R} = U \Sigma V^\dagger, \quad (49)$$

can be realized as follows:

$$U = \frac{1}{\sqrt{z+h}} \begin{pmatrix} \sqrt{z} & -\sqrt{h} & 0 \\ \sqrt{\frac{h}{2}} & \sqrt{\frac{z}{2}} & -\sqrt{\frac{z+h}{2}} \\ \sqrt{\frac{h}{2}} & \sqrt{\frac{z}{2}} & \sqrt{\frac{z+h}{2}} \end{pmatrix}, \quad (50)$$

$$\Sigma = \begin{pmatrix} \sqrt{z+h} \\ 0 \\ 0 \end{pmatrix}, \quad (51)$$

$$V = 1, \quad (52)$$

and the QE gauge fixing procedure above reduces to performing the following matrix multiplications:

$$\mathcal{R}' = U^\dagger \mathcal{R} = \begin{pmatrix} \sqrt{z+h} \\ 0 \\ 0 \end{pmatrix} \simeq \begin{pmatrix} 1 \\ 0 \\ 0 \end{pmatrix}, \quad (53)$$

$$\Lambda' = U^\dagger \Lambda U = \frac{-l}{\sqrt{z+h}} \begin{pmatrix} 0 & 0 & \sqrt{h} \\ 0 & 0 & \sqrt{z} \\ \sqrt{h} & \sqrt{z} & 0 \end{pmatrix},$$

$$\simeq -l \begin{pmatrix} 0 & 0 & \sqrt{h} \\ 0 & 0 & \sqrt{z} \\ \sqrt{h} & \sqrt{z} & 0 \end{pmatrix}, \quad (54)$$

where, in the last step of Eqs. (53) and (54), we used that $z + h = \Sigma^\dagger \Sigma \simeq 1$, consistently with the fact that the gGA framework captures both the quasiparticle weight and the Hubbard bands.

Therefore, the gauge transformation above reproduces the scenario represented in Fig. 1, featuring the same nonlocal

terms as the original Hamiltonian and additional ghost fermionic degrees of freedom interacting locally with each fragment. It is important to remember that as previously explained below Eq. (4), this reduction is exact only under the hypothesis that $\mathcal{R}^\dagger \mathcal{R} = z + h = 1$, which, while being satisfied accurately in gGA, is not met exactly.

As expected, the auxiliary degrees of freedom (corresponding to the first component of the above matrices) are decoupled from the auxiliary modes in the uncorrelated regime, where the spectral weight h of the Hubbard bands vanishes. On the other hand, such coupling becomes stronger as the interaction strength grows and, in the Mott phase, where the quasiparticle weight z vanishes, it becomes commensurate to $l \simeq \mathcal{U}$, where $\mathcal{U}$ is the Hubbard interaction strength of the model. This is consistent with the notion that $\hat{H}_*$, parametrized by $\mathcal{R}$ and Λ, serves as an effective Hamiltonian aiming to approximate the many-body interactions between the fragments and their respective environments with one-body operators. Consequently, it is natural that the ghost modes are useful only when many-body interactions are present.

IV. CONCLUSIONS

In this study, we derived the gDMET framework: a QE method based on principles that echo the foundational concepts underlying DMET, which is mathematically equivalent to the gGA. This reformulation offers an alternative, mathematically precise interpretation of the gGA equations and uncovers the underlying physical link between the two methods, besides introducing a practical advantage with a simpler implementation [72].

A key aspect of our analysis is the crucial role of the ghost degrees of freedom in connecting the DMET and gGA perspectives, i.e., their necessity for formulating a unified framework that adheres to the principles of both approaches. In relation to this point, it is interesting to note that as shown in Ref. [17], the limitations of standard GA in capturing charge fluctuations in the strongly correlated regime, particularly in the Mott phase, are directly tied to the method's inability to capture the entire spectral weight, and that the introduction of ghost degrees of freedom in gGA resolves these issues, providing results with accuracy that is essentially equal to DMFT. Our study suggests a possible association between the requirement of ghost degrees of freedom for achieving satisfactory accuracy and the feasibility of formulating the gGA equations also from a DMET perspective, contingent on the inclusion of ghost degrees of freedom.

Finally, the connection between gGA and DMET established here may pave the way for novel methodological generalizations, leveraging on the combined strengths of the variational perspective underlying the gGA framework and the QE perspective underlying DMET.

[1] P. R. C. Kent and G. Kotliar, Toward a predictive theory of correlated materials, Science **361**, 348 (2018).

[2] S. Qiming and G. Kin-Lic Chan, Quantum embedding theories, Acc. Chem. Res. **49**, 2705 (2016).

[3] A. Georges, G. Kotliar, W. Krauth, and M. J. Rozenberg, Dynamical mean-field theory of strongly correlated fermion systems and the limit of infinite dimensions, Rev. Mod. Phys. **68**, 13 (1996).

[4] V. Anisimov and Y. Izyumov, *Electronic Structure of Strongly Correlated Materials* (Springer, New York, 2010).

[5] K. Held, A. Nekrasov, G. Keller, V. Eyert, N. Blümer, A. K. McMahan, R. T. Scalettar, Th. Pruschke, V. I. Anisimov, and D. Vollhardt, Realistic investigations of correlated electron systems with LDA+DMFT, Phys. Stat. Sol. B **243**, 2599 (2006).

[6] V. I. Anisimov, A. I. Oteryaev, M. A. Korotin, A. O. Anokhin, and G. Kotliar, First-principles calculations of the electronic structure and spectra of strongly correlated systems: Dynamical mean-field theory, J. Phys.: Condens. Matter **9**, 7359 (1997).

[7] G. Kotliar, S. Y. Savrasov, K. Haule, V. S. Oudovenko, O. Parcollet, and C. A. Marianetti, Electronic structure calculations with dynamical mean-field theory, Rev. Mod. Phys. **78**, 865 (2006).

[8] M. C. Gutzwiller, Correlation of electrons in a narrow *s* band, Phys. Rev. **137**, A1726 (1965).

[9] W. Metzner and D. Vollhardt, Correlated lattice fermions in $d = \infty$ dimensions, Phys. Rev. Lett. **62**, 324 (1989).

[10] X.-Y. Deng, L. Wang, X. Dai, and Z. Fang, Local density approximation combined with Gutzwiller method for correlated electron systems: Formalism and applications, Phys. Rev. B **79**, 075114 (2009).

[11] K. M. Ho, J. Schmalian, and C. Z. Wang, Gutzwiller density functional theory for correlated electron systems, Phys. Rev. B **77**, 073101 (2008).

[12] N. Lanatà, H. U. R. Strand, X. Dai, and B. Hellsing, Efficient implementation of the Gutzwiller variational method, Phys. Rev. B **85**, 035133 (2012).

[13] N. Lanatà, Y. X. Yao, C.-Z. Wang, K.-M. Ho, and G. Kotliar, Phase diagram and electronic structure of praseodymium and plutonium, Phys. Rev. X **5**, 011008 (2015).

[14] J. Bünemann, F. Gebhard, T. Ohm, S. Weiser, and W. Weber, Gutzwiller-correlated wave functions: application to ferromagnetic nickel, in *Frontiers in Magnetic Materials*, edited by A. V. Narlikar (Springer, Berlin, 2005), pp. 117.

[15] C. Attaccalite and M. Fabrizio, Properties of Gutzwiller wave functions for multiband models, Phys. Rev. B **68**, 155117 (2003).

[16] N. Lanatà, T.-H. Lee, Y.-X. Yao, and V. Dobrosavljević, Emergent Bloch excitations in Mott matter, Phys. Rev. B **96**, 195126 (2017).

[17] M. S. Frank, T.-H. Lee, G. Bhattacharyya, P. K. H. Tsang, V. L. Quito, V. Dobrosavljević, O. Christiansen, and N. Lanatà, Quantum embedding description of the Anderson lattice model with the ghost Gutzwiller approximation, Phys. Rev. B **104**, L081103 (2021).

[18] D. Guerci, M. Capone, and M. Fabrizio, Exciton Mott transition revisited, Phys. Rev. Mater. **3**, 054605 (2019).

[19] F. Lechermann, A. Georges, G. Kotliar, and O. Parcollet, Rotationally invariant slave-boson formalism and momentum dependence of the quasiparticle weight, Phys. Rev. B **76**, 155102 (2007).

[20] T. Li, P. Wölfle, and P. J. Hirschfeld, Spin-rotation-invariant slave-boson approach to the Hubbard model, Phys. Rev. B **40**, 6817 (1989).

[21] N. Lanatà, Y. Yao, X. Deng, V. Dobrosavljević, and G. Kotliar, Slave boson theory of orbital differentiation with crystal field effects: Application to UO_2, Phys. Rev. Lett. **118**, 126401 (2017).

[22] L. de'Medici, A. Georges, and S. Biermann, Orbital-selective Mott transition in multiband systems: Slave-spin representation and dynamical mean-field theory, Phys. Rev. B **72**, 205124 (2005).

[23] R. Yu and Q. Si, $u(1)$ slave-spin theory and its application to Mott transition in a multiorbital model for iron pnictides, Phys. Rev. B **86**, 085104 (2012).

[24] G. Knizia and G. Kin-Lic Chan, Density matrix embedding: A simple alternative to dynamical mean-field theory, Phys. Rev. Lett. **109**, 186404 (2012).

[25] G. Knizia and G. K.-L. Chan, Density matrix embedding: A strong-coupling quantum embedding theory, J. Chem. Theory Comput. **9**, 1428 (2013).

[26] I. W. Bulik, G. E. Scuseria, and J. Dukelsky, Density matrix embedding from broken symmetry lattice mean fields, Phys. Rev. B **89**, 035140 (2014).

[27] U. Mordovina, T. E. Reinhard, I. Theophilou, H. Appel, and A. Rubio, Self-consistent density-functional embedding: A novel approach for density-functional approximations, J. Chem. Theory Comput. **15**, 5209 (2019).

[28] S. Sekaran, M. Saubanére, and E. Fromager, Local potential functional embedding theory: A self-consistent flavor of density functional theory for lattices without density functionals, Computation **10**, 45 (2022).

[29] S. Sekaran, M. Tsuchiizu, M. Saubanère, and E. Fromager, Householder-transformed density matrix functional embedding theory, Phys. Rev. B **104**, 035121 (2021).

[30] S. Yalouz, S. Sekaran, E. Fromager, and M. Saubanére, Quantum embedding of multi-orbital fragments using the block-householder transformation, J. Chem. Phys. **157**, 214112 (2022).

[31] S. Sekaran, O. Bindech, and E. Fromager, A unified density-matrix functional construction of quantum baths in density matrix embedding theory beyond the mean-field approximation, J. Chem. Phys. **159**, 034107 (2023).

[32] B.-X. Zheng, Density matrix embedding theory and strongly correlated lattice systems, Ph.D. thesis, Princeton University, 2017; arXiv:1803.10259.

[33] E. Fertitta and G. H. Booth, Rigorous wave function embedding with dynamical fluctuations, Phys. Rev. B **98**, 235132 (2018).

[34] P. V. Sriluckshmy, M. Nusspickel, E. Fertitta, and G. H. Booth, Fully algebraic and self-consistent effective dynamics in a static quantum embedding, Phys. Rev. B **103**, 085131 (2021).

[35] F. Verstraete, V. Murg, and J. I. Cirac, Matrix product states, projected entangled pair states, and variational renormalization group methods for quantum spin systems, Adv. Phys. **57**, 143 (2008).

[36] Y.-H. Zhang and S. Sachdev, From the pseudogap metal to the Fermi liquid using ancilla qubits, Phys. Rev. Res. **2**, 023172 (2020).

[37] J. Robledo Moreno, G. Carleo, A. Georges, and J. Stokes, Fermionic wave functions from neural-network constrained hidden states, Proc. Natl. Acad. Sci. **119**, e2122059119 (2022).

[38] S. Sakai, M. Civelli, and M. Imada, Hidden-fermion representation of self-energy in pseudogap and superconducting states of the two-dimensional Hubbard model, Phys. Rev. B **94**, 115130 (2016).

[39] P. W. Anderson, Hidden Fermi liquid: The secret of high-T_c cuprates, Phys. Rev. B **78**, 174505 (2008).

[40] T.-H. Lee, N. Lanatà, and G. Kotliar, Accuracy of ghost rotationally invariant slave-boson and dynamical mean field theory as a function of the impurity-model bath size, Phys. Rev. B **107**, L121104 (2023).

[41] C. Mejuto-Zaera and M. Fabrizio, Efficient computational screening of strongly correlated materials: Multiorbital phenomenology within the ghost Gutzwiller approximation, Phys. Rev. B **107**, 235150 (2023).

[42] G. Kotliar and A. E. Ruckenstein, New functional integral approach to strongly correlated Fermi systems: The Gutzwiller approximation as a saddle point, Phys. Rev. Lett. **57**, 1362 (1986).

[43] J. Bünemann and F. Gebhard, Equivalence of Gutzwiller and slave-boson mean-field theories for multiband Hubbard models, Phys. Rev. B **76**, 193104 (2007).

[44] N. Lanatà, P. Barone, and M. Fabrizio, Fermi-surface evolution across the magnetic phase transition in the Kondo lattice model, Phys. Rev. B **78**, 155127 (2008).

[45] N. Lanatà, Operatorial formulation of the ghost rotationally invariant slave-boson theory, Phys. Rev. B **105**, 045111 (2022).

[46] S. R. White, Density matrix formulation for quantum renormalization groups, Phys. Rev. Lett. **69**, 2863 (1992).

[47] J. Tilly, H. Chen, S. Cao, D. Picozzi, K. Setia, Y. Li, E. Grant, L. Wossnig, I. Rungger, G. H. Booth, and J. Tennyson, The variational quantum eigensolver: A review of methods and best practices, Phys. Rep. **986**, 1 (2022).

[48] Y. Yao, F. Zhang, C.-Z. Wang, K.-M. Ho, and P. P. Orth, Gutzwiller hybrid quantum-classical computing approach for correlated materials, Phys. Rev. Res. **3**, 013184 (2021).

[49] J. Rogers, T. Jiang, M. S. Frank, O. Christiansen, Y.-X. Yao, and N. Lanatà, Error mitigation in variational quantum eigensolvers using tailored probabilistic machine learning, arXiv:2111.08814.

[50] R. J. Bartlett and M. Musiał, Coupled-cluster theory in quantum chemistry, Rev. Mod. Phys. **79**, 291 (2007).

[51] N. Lanatà, Y.-X. Yao, X. Deng, C.-Z. Wang, K.-M. Ho, and G. Kotliar, Gutzwiller renormalization group, Phys. Rev. B **93**, 045103 (2016).

[52] T. Ayral, T.-H. Lee, and G. Kotliar, Dynamical mean-field theory, density-matrix embedding theory, and rotationally invariant slave bosons: A unified perspective, Phys. Rev. B **96**, 235139 (2017).

[53] T.-H. Lee, T. Ayral, Y.-X. Yao, N. Lanatà, and G. Kotliar, Rotationally invariant slave-boson and density matrix embedding theory: Unified framework and comparative study on the one-dimensional and two-dimensional Hubbard model, Phys. Rev. B **99**, 115129 (2019).

[54] T. Ayral, S. Biermann, and P. Werner, Screening and nonlocal correlations in the extended hubbard model from self-consistent combined *gw* and dynamical mean field theory, Phys. Rev. B **87**, 125149 (2013).

[55] H. Terletska, T. Chen, and E. Gull, Charge ordering and correlation effects in the extended hubbard model, Phys. Rev. B **95**, 115149 (2017).

[56] G. Rohringer, H. Hafermann, A. Toschi, A. A. Katanin, A. E. Antipov, M. I. Katsnelson, A. I. Lichtenstein, A. N. Rubtsov, and K. Held, Diagrammatic routes to nonlocal correlations beyond dynamical mean field theory, Rev. Mod. Phys. **90**, 025003 (2018).

[57] R. Chitra and G. Kotliar, Effect of long range Coulomb interactions on the Mott transition, Phys. Rev. Lett. **84**, 3678 (2000).

[58] G. Goldstein, N. Lanatà, and G. Kotliar, Extending the Gutzwiller approximation to intersite interactions, Phys. Rev. B **102**, 045152 (2020).

[59] N. Lanatà, Local bottom-up effective theory of nonlocal electronic interactions, Phys. Rev. B **102**, 115115 (2020).

[60] W.-S. Wang, X.-M. He, D. Wang, Q.-H. Wang, Z. D. Wang, and F. C. Zhang, Finite-temperature Gutzwiller projection for strongly correlated electron systems, Phys. Rev. B **82**, 125105 (2010).

[61] M. Sandri, M. Capone, and M. Fabrizio, Finite-temperature Gutzwiller approximation and the phase diagram of a toy model for V_2O_3, Phys. Rev. B **87**, 205108 (2013).

[62] N. Lanatà, X. Deng, and G. Kotliar, Finite-temperature Gutzwiller approximation from the time-dependent variational principle, Phys. Rev. B **92**, 081108(R) (2015).

[63] C. Sun, U. Ray, Z.-H. Cui, M. Stoudenmire, M. Ferrero, and Garnet Kin-Lic Chan, Finite-temperature density matrix embedding theory, Phys. Rev. B **101**, 075131 (2020).

[64] G. Seibold and J. Lorenzana, Time-dependent Gutzwiller approximation for the Hubbard model, Phys. Rev. Lett. **86**, 2605 (2001).

[65] M. Schiró and M. Fabrizio, Time-dependent mean field theory for quench dynamics in correlated electron systems, Phys. Rev. Lett. **105**, 076401 (2010).

[66] N. Lanatà and H. U. R. Strand, Time-dependent and steady-state Gutzwiller approach for nonequilibrium transport in nanostructures, Phys. Rev. B **86**, 115310 (2012).

[67] D. Guerci, M. Capone, and N. Lanatà, Time-dependent ghost-Gutzwiller nonequilibrium dynamics, Phys. Rev. Res. **5**, L032023 (2023).

[68] D. Jaksch, V. Venturi, J. I. Cirac, C. J. Williams, and P. Zoller, Creation of a molecular condensate by dynamically melting a Mott insulator, Phys. Rev. Lett. **89**, 040402 (2002).

[69] M. Yan, H.-Y. Hui, M. Rigol, and V. W. Scarola, Equilibration dynamics of strongly interacting bosons in 2D lattices with disorder, Phys. Rev. Lett. **119**, 073002 (2017).

[70] M. Yan, H.-Y. Hui, and V. W. Scarola, Dynamics of disordered states in the Bose-Hubbard model with confinement, Phys. Rev. A **95**, 053624 (2017).

[71] J. S. Kretchmer and G. K.-L. Chan, A real-time extension of density matrix embedding theory for nonequilibrium electron dynamics, J. Chem. Phys. **148**, 054108 (2018).

[72] See Supplemental Material at http://link.aps.org/supplemental/10.1103/PhysRevB.108.235112 for the following: Proof of theorem used in Sec. II B; standard derivation of gGA equations; proof of equivalence between gGA and the gDMET equations, derived in the main from QE principles; derivation of gDMET equations in momentum representation, for systems with translational symmetry. This includes a Ref. [73].

[73] R. Frésard and P. Wölfle, Unified slave boson representation of spin and charge degrees of freedom for strongly correlated Fermi systems, Intl. J. Mod. Phys. B **06**, 685704 (1992).

[74] S. Wouters, C. A. Jiménez-Hoyos, Q. Sun, and G. K.-L. Chan, A practical guide to density matrix embedding theory in quantum chemistry, J. Chem. Theory Comput. **12**, 2706 (2016).